



This is the peer-reviewed author-version of:

A liquid alkoxide precursor for the atomic layer deposition of aluminum oxide films

Reference

L. Cao, F. Mattelaer, T. Sajavaara, J. Dendooven and C. Detavernier, *J. Vac. Sci. Technol. A* **38** (2), 6 (2020).

Full text (Publisher's DOI): <https://doi.org/10.1116/1.5139631>

A liquid alkoxide precursor for the atomic layer deposition of aluminum films

Running title: A liquid alkoxide precursor ATSB for ALD of Al₂O₃ thin films

Running Authors: Cao et al.

LiAo Cao ^{1,a)}, Felix Mattelaer ¹, Timo Sajavaara ², Jolien Dendooven ¹,
Christophe Detavernier ¹

¹Department of Solid State Science, Ghent University, Belgium

²Department of Physics, University of Jyväskylä, Finland

a) Electronic mail: LiAo.Cao@UGent.be

For large scale atomic layer deposition of alumina, the most commonly used alkyl precursor trimethylaluminum poses safety issues due to its pyrophoric nature. In this work, we have investigated a liquid alkoxide, aluminum tri-sec-butoxide (ATSB), as precursor for ALD deposition of alumina. ATSB is thermally stable and the liquid nature facilitates handling in a bubbler and potentially enables liquid injection towards upscaling. Both thermal and plasma enhanced ALD processes are investigated in a vacuum type reactor by using water, oxygen plasma and water plasma as co-reactants. All processes achieved ALD deposition at a growth rate of 1-1.4 Å/cycle for substrate temperatures ranging from 100 °C to 200 °C. Film morphology, surface roughness and composition have been studied with different characterization techniques.

I. INTRODUCTION

Aluminum oxide films are widely investigated due to their excellent chemical and thermal stability, high transparency, high breakdown voltage and high resistivity. They are used as encapsulation layers¹⁻³, barrier materials^{4,5} and dielectric films^{6,7}. In such applications, coating a thin layer of aluminum oxide can suffice because of the excellent properties of these films. Among many commonly used methods for coating thin films, atomic layer deposition (ALD) can give excellent control of film thickness, stoichiometry and conformality by a series of self-limited reactions⁸. Since the technique was first commercially used in depositing conformal ultra-thin films for electro-luminescent displays and microelectronics applications, more attention is drawn towards other applications, such as photovoltaics⁹⁻¹¹, flexible electronics¹² and powder coating¹³. Recent progress in reactor and process design ensure that large-area ALD is possible for those applications¹⁴⁻¹⁶. Compared to typical precursor consumption of ALD processes during microelectronics fabrication, the implementation of large-area ALD will increase precursor usage with a factor of 100 for roll-to-roll applications and up to 4 orders of magnitude for powder coatings, depending on the total volume of the powder bed¹⁷. Thus, safety for use and large-scale storage as well as a reasonable cost are essential requirements for precursors used in large-area applications.

Trimethylaluminum (TMA) and its thermal process with water is the most commonly used precursor and process for ALD deposition of aluminum oxide¹⁸⁻²³. TMA is a highly volatile and thermally stable chemical and its high reactivity makes it an ideal precursor for ALD deposition with different co-reactants over a wide range of temperatures. However, due to the direct metal-carbon bonding in the TMA molecule, TMA is also pyrophoric, toxic, corrosive and moisture sensitive, which makes handling

inconvenient. Many efforts have been done to search for alternatives to TMA in ALD of aluminum oxide. $\text{Me}_2\text{AlO}^i\text{Pr}$,^{24,25} $[\text{MeC}(\text{N}^i\text{Pr})_2]\text{AlEt}_2$,²⁶ AlCl_3 ,²⁷⁻³⁰ AlEt_3 ³¹ and Me_2AlCl ^{32,33} have been investigated during the past years. However, most of these alternative precursors can still rise safety, contamination and cost problems in large-area applications.

Alkoxide precursors^{34,35} can be a non-pyrophoric alternative to alkyls, as they only possess metal-oxygen bonds, not metal-carbon bonds. These chemicals have moderate thermal stability but are highly cost-effective when aiming to large scale use. Alkoxide precursors, such as aluminum tri-isopropoxide (TIPA) and aluminum tri-ethoxide (TEA) have been studied and used in chemical vapor deposition (CVD)^{36,37}. Recently, we reported using TIPA as aluminum source for ALD deposition of aluminum oxide³⁸. Water, oxygen plasma and water plasma were used as oxygen source and the processes generated high growth-per-cycle and conformal thin films. However, TIPA is a solid precursor and it requires high source temperature to generate enough vapor into the reactor chamber for deposition. Though described as mildly toxic, aluminum tri-sec-butoxide (ATSB) is a stable liquid alkoxide precursor³⁹. Its liquid nature suggests that it could be easier to generate enough vapor pressure at lower source temperature and could facilitate liquid injection for large-area applications^{40,41} when very high precursor dosing is required. A recent paper researched ATSB for CVD and ALD deposition⁴². However, in that work, no ALD parameters such as saturation and temperature windows were reported and only the thermal process was reported.

In this work, we have performed an in-depth study on the (PE)ALD process characteristics and film properties using ATSB as a precursor. During thermal and

plasma processes, we observe an apparent ALD growth window for Al_2O_3 from 100°C up to 300°C . The growth rates achieved within the ALD window for all investigated processes are comparable to the typical rate that is achieved for thermal ALD using TMA and water ($1.1\text{\AA}/\text{cycle}$). However, it is also found that ATSB starts to decompose from 200°C , although the decomposition rate appears quite limited for typical exposure doses until 300°C . Scanning electron microscopy and atomic force microscopy images indicate a smooth surface of the deposited films from all processes. X-ray photoelectron spectroscopy analysis confirms stoichiometric deposition of Al_2O_3 with carbon contamination below XPS detection limits (about 0.5 at. %) when an oxygen plasma was applied and only 1-2 at. % carbon for low-temperature H_2O -based thermal processes. The time-of-flight elastic recoil detection (ToF-ERD) confirms the presence of carbon impurities in the films deposited through thermal ALD and indicates varying degrees of hydrogen content in the deposited films depending on the process condition.

II. EXPERIMENTAL

A home-built pump-type ALD reactor⁴³ is used for the process development of ATSB and several different reactants. ATSB was bought from Sigma-Aldrich with 97% purity. A glass bubbler with a stainless-steel lid was used to contain the liquid ATSB and water was stored in a stainless-steel bottle. To generate sufficient vapor pressure, the water bottle was kept at room temperature, but the conveying line was heated to 80°C in order to avoid condensation. The bubbler containing ATSB was heated until 100°C to generate sufficient precursor vapor and the transporting line was heated to 105°C to avoid condensation. Argon gas was pulsed into the bubbler to carry precursor vapor into the reactor. Water, oxygen plasma and water plasma were used as reactants in three

deposition processes. A fused quartz column wrapped by a copper coil was placed on top of the chamber to generate plasma by connecting to a 13.56 MHz RF generator (ENI GHW-12Z). The remote plasma was set at 200W and generated with an impedance matching network to minimize the reflected power.

The substrates used for deposition were Si (100) wafers with native oxide and cleaned by oxygen plasma to remove surface contamination before a process was started. During deposition, the Si substrate was placed on a copper block and heated evenly at a temperature varied from 100°C to 300°C. The pressure of the precursor pulse was controlled at 5×10^{-3} mbar with the turbo pump running. The pressure during the plasma pulse was also controlled at 5×10^{-3} mbar.

During deposition, a spectroscopic ellipsometry [(SE) J.A. Woollam M-200] was attached on the reactor to monitor aluminum oxide film growth in-situ. The results were fitted with a Cauchy model for Al_2O_3 and the model parameters were optimized by inputting the final thickness of Al_2O_3 oxide films measured ex-situ with X-ray reflectivity (XRR). A Bruker D8 diffractometer using Cu K- α radiation was used to obtain XRR patterns. By fitting simulated patterns to measured ones, the analyses of the XRR patterns gave the information of the thickness and the films density. Films of about 20-30 nm thick deposited with water and plasma processes in 200 cycles were characterized by different methods. Scanning electron microscopy (SEM) was performed for surface imaging by a FEI Quanta 200F setup with a 10 keV electron beam energy. The surface morphology was determined by atomic force microscopy (AFM) with a Bruker Dimension Edge system operating in tapping mode in air. X-ray photoelectron spectroscopy (XPS) was conducted by using a Theta Probe system from Thermo

Scientific using Al K α X-rays generated at 15kV and focusing to a spot size of 0.3 mm by an MXR1 monochromator gun to analyze chemical composition of the films. Film samples were cleaned and etched by a short Ar plasma treatment to remove the surface carbon contamination and obtain the elemental depth profile during the XPS measurement. ToF-ERD was performed using a home-built spectrometer and a 1.7 MV Pelletron accelerator in Jyväskylä⁴⁴. The incident particle beam for these measurements consisted of 11.915 MeV ⁶³Cu⁶⁺ ions at an incoming angle of 10° and total scattering angle of 41°. The collected spectra were analyzed using in-house developed open source software called Potku⁴⁵.

III. RESULTS AND DISCUSSION

To generate sufficient precursor vapor, the glass bubbler containing the ATSB was heated to 100 °C. Three co-reactants were examined to react with the chemisorbed ATSB to generate deposition, i.e. water, oxygen plasma and water plasma. In-situ ellipsometry results confirmed linear growth as a function of the number of ALD cycles for all three processes when the sample temperature was 150 °C, as shown in Fig. 1[a]. The dosing of ATSB was 15 seconds and the dosing time of the co-reactants was 5s.

The processes were further investigated at various substrate temperatures, from 100 °C to 400 °C. To examine the presence of an unwanted CVD component, a process was run also without co-reactant. The growth per cycle (GPC) of the three processes and decomposition by only pulsing ATSB vapor are shown in Fig. 1[b], as a function of temperature. The dosing time was the same as that used in the linear growth tests. Based on the GPC values, the temperature range could be divided into three regions. At low temperature, no decomposition of ATSB is observed and the GPC of the three processes

is stable around 1-1.4 Å/cycle. In this region, the deposition is generated only by self-limiting surface reaction of ATSB and co-reactants. When the substrate is heated above 200 °C, the GPC behavior enters region II. The GPC of the ATSB and co-reactants processes is still stable, but decomposition of ATSB is also initiated. This means, by a typical ATSB dosing time of 15s, the decomposition is quite limited compared to the reaction with co-reactants. Haanappel et al.^{46,47} reported that from a temperature of 190°C the decomposition of ATSB is decomposing dominated by a β -hydride elimination mechanism and that a trace amount of water can contribute to the decomposition at high temperature. However, when we further increased the substrate temperature over 300 °C, the decomposition rate of ATSB takes off. The GPC in region III increased as the temperature increased and coincided with that of decomposition. In this region, the deposition on the substrate is dominated by the decomposition of ATSB.

To ensure the reaction in region I is a self-limited ALD deposition, the saturation behavior of both ATSB precursor and co-reactants were investigated at the substrate temperature of 150 °C. Firstly, the precursor test was done with 5s co-reactants pulse and the saturation (Fig. 2[a]) was achieved after a few seconds ATSB vapor pulse. Then, fixing the ATSB pulse time as 15s, the growth was also saturated (Fig. 2[b]) after 1s co-reactant pulse. The thermal process using water and the two plasma processes had a similar saturation behavior and the results indicate that the deposition in region I is indeed ALD growth. The same saturation tests were also carried out at 275 °C (region II), as shown in Fig. 3. At this temperature saturation could not be achieved (Fig. 3[a]) and the GPC kept increasing with longer precursor pulses, regardless of the co-reactant species. When the precursor pulse time was fixed at 15 seconds, there was already some

growth without involving any co-reactants (Fig. 3[b]) due to the decomposition. The GPC increased when water or plasma was applied into the deposition and saturated, which is similar with the behavior of the co-reactant pulse at 150 °C.

To investigate the quality of the films deposited by thermal and plasma ALD processes using ATSB, SEM and AFM studies were conducted on the films deposited at 150 °C substrate temperature. The results confirmed the deposition of smooth and uniform films when oxygen plasma (Fig. 4[a] and 4[d]), water plasma (Fig. 4[b] and 4[e]) and water (Fig. 4[c] and 4[e]) were used as co-reactant with ATSB. The root mean square (RMS) roughness was calculated from the AFM data and varied in value of 0.3~0.5 nm for all samples, indicating smooth layers.

To investigate the composition of the aluminum oxide films deposited in region I and II, XPS was carried out on samples deposited with three co-reactants at substrate temperatures of 100 °C, 150 °C and 275 °C. As shown in Fig. 5[a] and Fig. 5[b], Al and O signals indicate the deposition of an alumina film. The carbon peak from the as-deposited film disappeared after Ar plasma etching the surface, suggesting that only a small content of carbon is present in the films. However, when we look closely to the carbon peak position after etching, a very weak carbon peak was still there (Fig. 5[c]) for samples grown with the water thermal process at 100 °C and 150 °C. The spectra near the carbon position after etching are shown in Fig. 6 for samples in five deposition conditions, i.e. the thermal process at 100 °C, 150 °C and 275 °C and the PE-ALD process at 150 °C. The figure shows that carbon is indeed present in the thermally grown films using water at low temperature, i.e. at 100 °C and 150 °C. The XPS measured concentration of carbon in the water-thermal process sample at 100 °C and 150 °C was approximately 0.5 at. %,

which is near the detection limit of XPS. The position of the carbon peak is around 289.3 eV⁴⁸ and can be signed to C-O bonds. The result indicates that at low temperature water molecule is not active enough to replace all the alkoxy ligands of the precursor. In the ALD regime in region I by using plasma as the co-reactant, no carbon was detected by XPS, indicating superior purity even at 100 °C within the ALD regime. Finally, when a higher temperature was used for the thermal process, i.e. 275 °C, in region II in Fig. 1[b], no carbon was detected. However, the reader must note that this process is no longer truly ALD, and the CVD component will challenge the conformality aspect of the films and limit the upscalability.

Since XPS cannot detect hydrogen, commonly found as an impurity in ALD films originating from remaining ligands or absorbed water, ToF-ERD was used to determine the hydrogen content and provide a more sensitive detection for light elements such as carbon and oxygen. Six samples were selected: water thermal ALD films at 150 °C, 200 °C and 275 °C and oxygen plasma ALD films at the same temperatures. As shown in Table I, ToF-ERD analysis confirms the low carbon content revealed by the XPS results. Thermal ALD film results in 0.7-1.3 at. % carbon content, depending on the deposition temperature. For plasma-based films, the carbon content is below the detection limit of ToF-ERD (<0.2 at. %) for this kind of below 30 nm thick films. A small amount of Ti was detected in the films. The Ti signal is most likely originating from contamination of the precursor conveying tube, since there is no Ti source in the ALD reaction system.



TABLE I. Atomic concentrations in the central region of the deposited films (conditions as below), not considering interface effects at the surface or silicon interface, as calculated from the ToF-ERD measurements using POTKU software

	O (at. %)	Al (at. %)	H (at. %)	C (at. %)	Ti (at. %)
H ₂ O ALD, 150 °C	53±4	25±3	19±2	1.3±0.3	0.9±0.2
H ₂ O ALD, 200 °C	54±3	29±2	17±2	0.7±0.2	0.4±0.1
H ₂ O ALD, 275 °C	60±4	36±3	1.9±0.5	0.8±0.3	0.7±0.2
O ₂ PE-ALD, 150 °C	58±3	32±2	8.2±0.8	<0.2	1.7±0.2
O ₂ PE-ALD, 200 °C	55±3	34±3	7.5-12.5	<0.2	0.9±0.1
O ₂ PE-ALD, 275 °C	59±3	34±3	6.1±1.0	<0.2	0.8±0.1

Furthermore, the hydrogen content in films from the plasma process is relatively stable from 8.2 to 6.1 at. % as the temperature increases. The oxygen plasma tends to combust all ligands, which leaves a very low carbon trace and some hydrogen residue. The combustion effect does not change as the temperature increases. The hydrogen content cannot originate from -CH₃ residue in the films, due to the low carbon content. This suggests that hydrogen is present in the film in the form of -OH groups or water molecules. While the stoichiometry of the films from the plasma process is close to what is expected for aluminum oxide with 60 at. % oxygen, the Al is slightly lower than 40 at. %. After subtracting the O amount for the -OH groups, based on the measured H, and Ti impurities, the Al:O ratio is indeed close to that of stoichiometric aluminum oxide. Surprisingly, there is even less hydrogen content in the thermal process with water at 275 °C. The reaction in region II may already go towards decomposition at 275 °C, supporting that during the decomposition hydrogen must be removed. However, for

thermal based samples in region I, a much higher hydrogen content (17-19 at. %) was observed. The carbon impurities in these films suggest the presence of $-CH_x$ groups and the C is from remaining alkoxy ligands according to the XPS analysis. But since the measured H:C ratio is larger than 3:1, $-OH$ groups are also present in these films. By assuming the C and H are present in these forms in the films, the corrected Al:O ratio is again in agreement with stoichiometric aluminum oxide.

IV. SUMMARY AND CONCLUSIONS

ATSB was demonstrated as a liquid, non-pyrophoric alkoxy-type precursor for ALD of aluminum oxide. Thermal ALD with water and plasma enhanced ALD with water plasma and oxygen plasma produced smooth, uniform and near-stoichiometric Al_2O_3 layers. The GPC of the three process was 1.0-1.4 Å/cycle from 100 °C to 300 °C. Detailed investigation of the saturation behavior and thermal decomposition of ATSB indicated real ALD conditions for substrate temperature of 100 °C to 200 °C, while some parasitic CVD-type decomposition occurred from 200 °C to 300 °C. For thermal ALD with H_2O as co-reactant, the films contained 0.7-1.3 at. % carbon contamination and 17-19 at. % hydrogen for deposition at 100 °C to 200 °C or 1.9 at. % hydrogen at 275 °C. For plasma enhanced ALD with O_2 plasma as co-reactant, the carbon contamination was below the detection limit of both XPS and ToF-ERD, while ERD indicated approximately 6.1-8.2 at. % hydrogen impurities.

ACKNOWLEDGMENTS

This work is supported by the M-ERA CALDERA project and the Fund for Scientific Research Flanders (FWO). Jolien Dendooven acknowledges the FWO for a post-doctoral fellowship.

- ¹ Y.Q. Yang, Y. Duan, P. Chen, F.B. Sun, Y.H. Duan, X. Wang, and D. Yang, *J. Phys. Chem. C* **117**, 20308 (2013).
- ² H.Y. Li, Y.F. Liu, Y. Duan, Y.Q. Yang, and Y.N. Lu, *Materials (Basel)*. **8**, 600 (2015).
- ³ Y. Liu, J. Tolentino, M. Gibbs, R. Ihly, C.L. Perkins, Y. Liu, N. Crawford, J.C. Hemminger, and M. Law, *Nano Lett.* **13**, 1578 (2013).
- ⁴ P. Poodt, A. Lankhorst, F. Roozeboom, K. Spee, D. Maas, and A. Vermeer, *Adv. Mater.* **22**, 3564 (2010).
- ⁵ L.J. Antila, M.J. Heikkilä, V. Mäkinen, N. Humalamäki, M. Laitinen, V. Linko, P. Jalkanen, J. Toppari, V. Aumanen, M. Kemell, P. Myllyperkiö, K. Honkala, H. Häkkinen, M. Leskelä, and J.E.I. Korppi-Tommola, *J. Phys. Chem. C* **115**, 16720 (2011).
- ⁶ J.H. Chang, D.Y. Choi, S. Han, and J.J. Pak, *Microfluid. Nanofluidics* **8**, 269 (2010).
- ⁷ M. Wang, X. Li, X. Xiong, J. Song, C. Gu, D. Zhan, Q. Hu, S. Li, and Y. Wu, *IEEE Electron Device Lett.* **40**, 419 (2019).
- ⁸ V. Cremers, R.L. Puurunen, and J. Dendooven, *Appl. Phys. Rev.* **6**, (2019).
- ⁹ T.R.B. Foong, Y. Shen, X. Hu, and A. Sellinger, *Adv. Funct. Mater.* **20**, 1390 (2010).
- ¹⁰ I.S. Kim, R.T. Haasch, D.H. Cao, O.K. Farha, J.T. Hupp, M.G. Kanatzidis, and A.B.F. Martinson, *ACS Appl. Mater. Interfaces* **8**, 24310 (2016).
- ¹¹ J.A. Van Delft, D. Garcia-Alonso, and W.M.M. Kessels, *Semicond. Sci. Technol.* **27**, (2012).
- ¹² P. Poodt, R. Knaapen, A. Illiberi, F. Roozeboom, and A. van Asten, *J. Vac. Sci. Technol. A Vacuum, Surfaces, Film.* **30**, 01A142 (2012).
- ¹³ B.J. Oneill, D.H.K. Jackson, J. Lee, C. Canlas, P.C. Stair, C.L. Marshall, J.W. Elam,

- T.F. Kuech, J.A. Dumesic, and G.W. Huber, *ACS Catal.* **5**, 1804 (2015).
- ¹⁴ D. Longrie, D. Deduytsche, and C. Detavernier, *J. Vac. Sci. Technol. A Vacuum, Surfaces, Film.* **32**, 010802 (2014).
- ¹⁵ H. Van Bui, F. Grillo, and J.R. Van Ommen, *Chem. Commun.* **53**, 45 (2017).
- ¹⁶ H. Tiznado, D. Domínguez, F. Muñoz-Muñoz, J. Romo-Herrera, R. Machorro, O.E. Contreras, and G. Soto, *Powder Technol.* **267**, 201 (2014).
- ¹⁷ E. Granneman, P. Fischer, D. Pierreux, H. Terhorst, and P. Zagwijn, *Surf. Coatings Technol.* **201**, 8899 (2007).
- ¹⁸ V. Miikkulainen, M. Leskelä, M. Ritala, and R.L. Puurunen, *J. Appl. Phys.* **113**, (2013).
- ¹⁹ S.M. George, *Chem. Rev.* **110**, 111 (2010).
- ²⁰ R.L. Puurunen, *J. Appl. Phys.* **97**, (2005).
- ²¹ M. Leskelä and M. Ritala, *Angew. Chemie - Int. Ed.* **42**, 5548 (2003).
- ²² M. Leskelä and M. Ritala, *Thin Solid Films* **409**, 138 (2002).
- ²³ S.M. George, A.W. Ott, and J.W. Klaus, *J. Phys. Chem.* **100**, 13121 (1996).
- ²⁴ W. Cho, K. Sung, K.-S. An, S. Sook Lee, T.-M. Chung, and Y. Kim, *J. Vac. Sci. Technol. A Vacuum, Surfaces, Film.* **21**, 1366 (2003).
- ²⁵ S.E. Potts, G. Dingemans, C. Lachaud, and W.M.M. Kessels, *J. Vac. Sci. Technol. A Vacuum, Surfaces, Film.* **30**, 021505 (2012).
- ²⁶ A.L. Brazeau and S.T. Barry, *Chem. Mater.* **20**, 7287 (2008).
- ²⁷ S. Dueñas, H. Castán, H. García, A. De Castro, L. Bailón, K. Kukli, A. Aidla, J. Aarik, H. Mändar, T. Uustare, J. Lu, and A. Hårsta, *J. Appl. Phys.* **99**, (2006).
- ²⁸ M. Ritala, H. Saloniemi, M. Leskelä, T. Prohaska, G. Friedbacher, and M.

- Grasserbauer, *Thin Solid Films* **286**, 54 (1996).
- ²⁹ S.J. Yun, K.-H. Lee, J. Sarp, H.-R. Kim, and K.-S. Nam, *J. Vac. Sci. Technol. A Vacuum, Surfaces, Film.* **15**, 2993 (1997).
- ³⁰ M. Tiitta, E. Nykänen, P. Soininen, L. Niinistö, M. Leskelä, and R. Lappalainen, *Mater. Res. Bull.* **33**, 1315 (1998).
- ³¹ R. Huang and A.H. Kitai, *Thin Film.* **22**, 215 (1993).
- ³² S. Li, Y. Bao, M. Laitinen, T. Sajavaara, M. Putkonen, and H. Savin, *Phys. Status Solidi Appl. Mater. Sci.* **212**, 1795 (2015).
- ³³ K. Kukli, M. Ritala, M. Leskelä, and J. Jokinen, *J. Vac. Sci. Technol. A Vacuum, Surfaces, Film.* **15**, 2214 (1997).
- ³⁴ D.C. Bradley and M.M. Faktor, *J. Appl. Chem.* **9**, 435 (1959).
- ³⁵ D.C. Bradley and J.M. Thomas, *Philos. Trans. R. Soc. A Math. Phys. Eng. Sci.* **330**, 167 (1990).
- ³⁶ S. Blittersdorf, N. Bahlawane, K. Kohse-Höinghaus, B. Atakan, and J. Müller, *Chem. Vap. Depos.* **9**, 194 (2003).
- ³⁷ L. Hiltunen, H. Kattelus, M. Leskelä, M. Mäkelä, L. Niinistö, E. Nykänen, P. Soininen, and M. Tiittad, *Mater. Chem. Phys.* **28**, 379 (1991).
- ³⁸ F.S.M. Hashemi, L. Cao, F. Mattelaer, T. Sajavaara, J.R. van Ommen, and C. Detavernier, *J. Vac. Sci. Technol. A* **37**, 040901 (2019).
- ³⁹ G.P. Shulman, M. Trusty, and J.H. Vickers, *J. Org. Chem.* **28**, 907 (1963).
- ⁴⁰ R.J. Potter, P.R. Chalker, T.D. Manning, H.C. Aspinall, Y.F. Loo, A.C. Jones, L.M. Smith, G.W. Critchlow, and M. Schumacher, *Chem. Vap. Depos.* **11**, 159 (2005).
- ⁴¹ P.R. Chalker, S. Romani, P.A. Marshall, M.J. Rosseinsky, S. Rushworth, and P.A.

This is the author's peer reviewed, accepted manuscript. However, the online version of record will be different from this version once it has been copyedited and typeset.
PLEASE CITE THIS ARTICLE AS DOI: 10.1116/1.5139631

- Williams, *Nanotechnology* **21**, (2010).
- ⁴² X. Xia, A. Taylor, Y. Zhao, S. Guldin, and C. Blackman, *Materials (Basel)*. **12**, (2019).
- ⁴³ T. Dobbelaere, F. Mattelaer, A.K. Roy, P. Vereecken, and C. Detavernier, *J. Mater. Chem. A* **5**, 330 (2017).
- ⁴⁴ M. Laitinen, M. Rossi, J. Julin, and T. Sajavaara, *Nucl. Instruments Methods Phys. Res. Sect. B Beam Interact. with Mater. Atoms* **337**, 55 (2014).
- ⁴⁵ K. Arstila, J. Julin, M.I. Laitinen, J. Aalto, T. Konu, S. Kärkkäinen, S. Rahkonen, M. Raunio, J. Itkonen, J.P. Santanen, T. Tuovinen, and T. Sajavaara, *Nucl. Instruments Methods Phys. Res. Sect. B Beam Interact. with Mater. Atoms* **331**, 34 (2014).
- ⁴⁶ V.A.C. Haanappel, H.D. van Corbach, T. Fransen, and P.J. Gellings, *Thermochim. Acta* **240**, 67 (1994).
- ⁴⁷ V.A.C. Haanappel, H.D. van Corbach, T. Fransen, and P.J. Gellings, *Thin Solid Films* **230**, 138 (1993).
- ⁴⁸ J.L. Hueso, J.P. Espinós, A. Caballero, J. Cotrino, and A.R. González-Elipe, *Carbon N. Y.* **45**, 89 (2007).

This is the author's peer reviewed, accepted manuscript. However, the online version of record will be different from this version once it has been copyedited and typeset.
PLEASE CITE THIS ARTICLE AS DOI: 10.1116/1.5139631

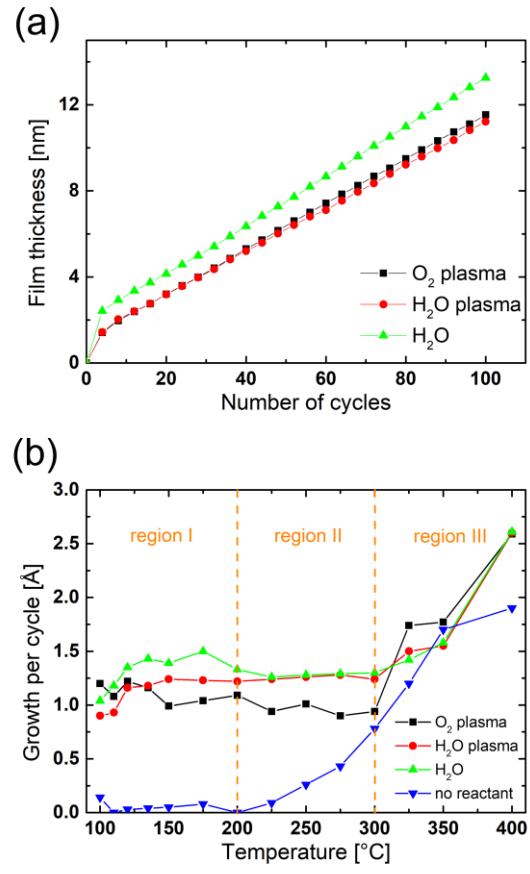


FIG. 1. (a) linear growth behavior on Si substrate at 150 °C, and (b) temperature windows of water, oxygen plasma and water plasma process.

This is the author's peer reviewed, accepted manuscript. However, the online version of record will be different from this version once it has been copyedited and typeset.
PLEASE CITE THIS ARTICLE AS DOI: 10.1116/1.5139631

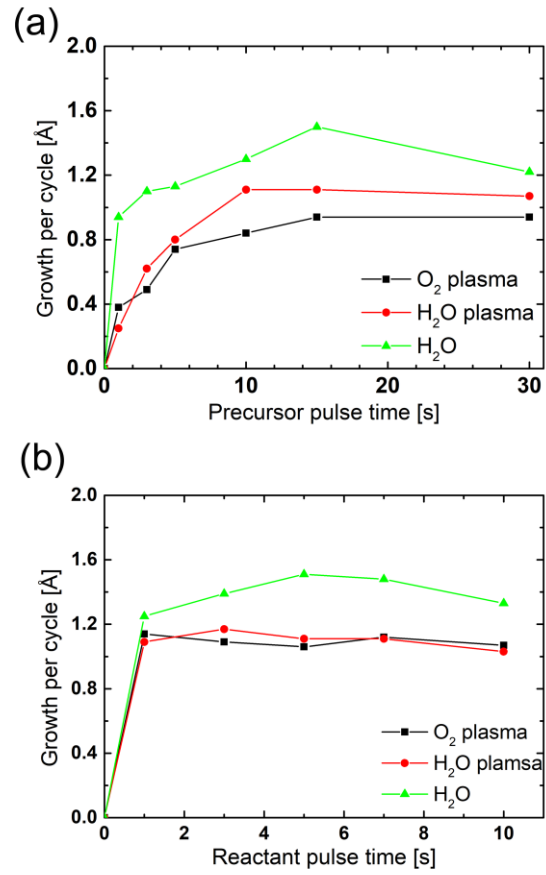


FIG. 2. Saturation curves at 150 °C, (a) 5s co-reactant pulse with different ATSB pulse time, and (b) 15s ATSB pulse with different pulse time for water, oxygen plasma and water plasma.

This is the author's peer reviewed, accepted manuscript. However, the online version of record will be different from this version once it has been copyedited and typeset.
PLEASE CITE THIS ARTICLE AS DOI: 10.1116/1.5139631

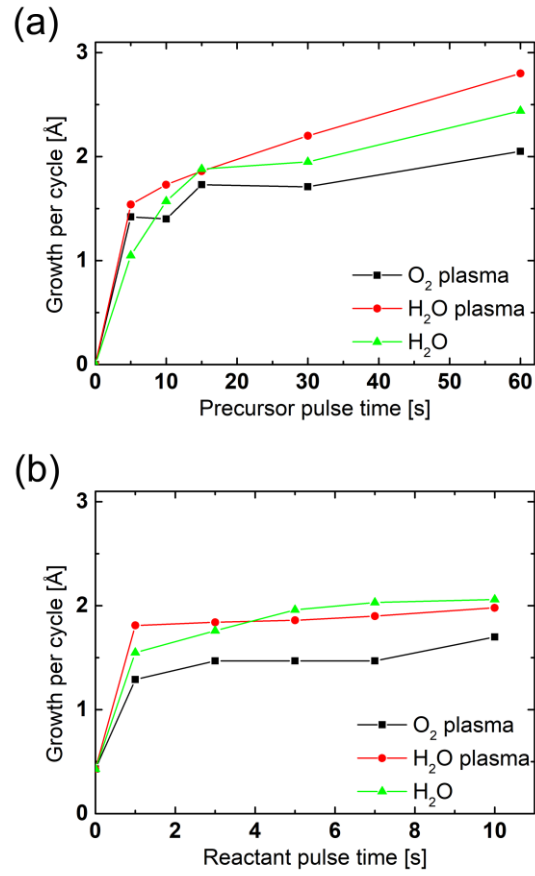


FIG. 3. Saturation curve at 275 °C, (a) 5s co-reactant pulse with different ATSB pulse time, and (b) 15s ATSB pulse with different pulse time for water, oxygen plasma and water plasma.

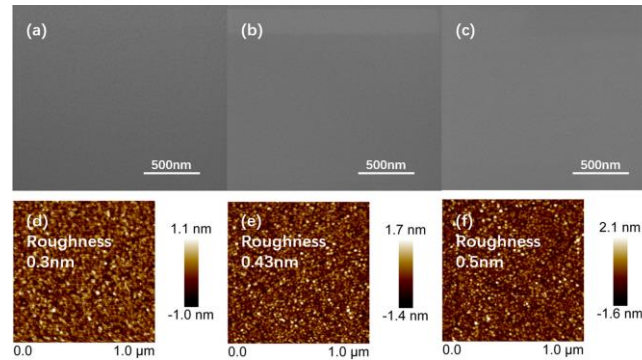


FIG. 4. SEM and AFM images of aluminum oxide films deposited at 150 °C using [(a) and (d)] oxygen plasma, [(b) and (e)] water plasma and [(c) and (f)] water as co-reactants.

This is the author's peer reviewed, accepted manuscript. However, the online version of record will be different from this version once it has been copyedited and typeset.
PLEASE CITE THIS ARTICLE AS DOI: 10.1116/1.5139631

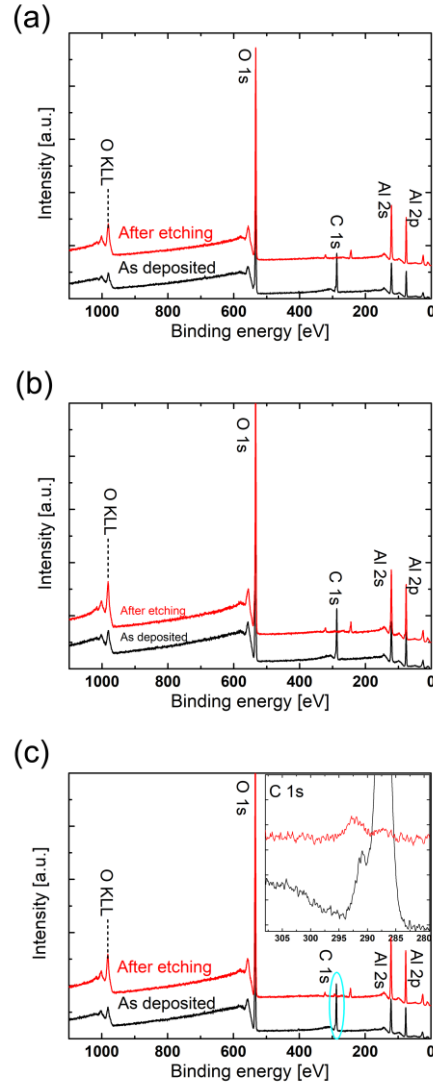


FIG. 5. XPS spectra of aluminum oxide films deposited at 150 °C with (a) oxygen plasma, (b) water plasma and (c) water as co-reactants

This is the author's peer reviewed, accepted manuscript. However, the online version of record will be different from this version once it has been copyedited and typeset.
PLEASE CITE THIS ARTICLE AS DOI: 10.1116/1.5139631

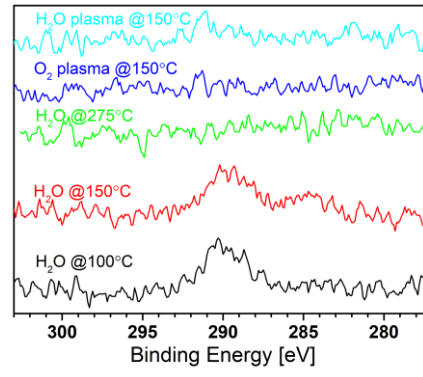


FIG. 6. The carbon details from XPS spectra of films deposited at different temperature with different co-reactants.